Heliyon 9 (2023) e17314

Contents lists available at ScienceDirect

Heliyon

journal homepage: www.cell.com/heliyon

Plexin D1 mediates disturbed flow-induced M1 macrophage polarization in atherosclerosis

Suhui Zhang [a,b,1], Yingqian Zhang [b,1], Peng Zhang [c,1], Zechen Wei [d,e,1], Mingrui Ma [a,b], Wei Wang [b], Wei Tong [b], Feng Tian [b], Hui Hui [d,e,***], Jie Tian [d,f,g,**], Yundai Chen [b,*]

[a] *Medical School of Chinese PLA, Chinese PLA General Hospital, Beijing, 100853, China*
[b] *Senior Department of Cardiology, The Sixth Medical Center of PLA General Hospital, Beijing, 100048, China*
[c] *School of Computer and Information Technology, Beijing Jiaotong University, Beijing, 100044, China*
[d] *CAS Key Laboratory of Molecular Imaging, Beijing Key Laboratory of Molecular Imaging, Institute of Automation, Chinese Academy of Sciences, Beijing, 100190, China*
[e] *University of Chinese Academy of Sciences, Beijing, 100080, China*
[f] *Key Laboratory of Big Data-Based Precision Medicine (Beihang University), Ministry of Industry and Information Technology of China, Beijing, 100191, China*
[g] *Zhuhai Precision Medical Center, Zhuhai People's Hospital, Affiliated with Jinan University, Zhuhai, 519000, China*

ARTICLE INFO

Keywords:
Plexin D1
Macrophage polarization
Disturbed flow
Bifurcation lesions
Atherosclerosis

ABSTRACT

Atherosclerosis preferentially develops at bifurcations exposed to disturbed flow. Plexin D1 (PLXND1) responds to mechanical forces and drives macrophage accumulation in atherosclerosis. Here, multiple strategies were used to identify the role of PLXND1 in site-specific atherosclerosis. Using computational fluid dynamics and three-dimensional light-sheet fluorescence-microscopy, the elevated PLXND1 in M1 macrophages was mainly distributed in disturbed flow area of ApoE$^{-/-}$ carotid bifurcation lesions, and visualization of atherosclerosis *in vivo* was achieved by targeting PLXND1. Subsequently, to simulate the microenvironment of bifurcation lesions *in vitro*, we co-cultured oxidized low-density lipoprotein (oxLDL)-treated THP-1-derived macrophages with shear-treated human umbilical vein endothelial cells (HUVECs). We found that oscillatory shear induced the increase of PLXND1 in M1 macrophages, and knocking down PLXND1 inhibited M1 polarization. Semaphorin 3E, the ligand of PLXND1 which was highly expressed in plaques, strongly enhanced M1 macrophage polarization via PLXND1 *in vitro*. Our findings provide insights into pathogenesis in site-specific atherosclerosis that PLXND1 mediates disturbed flow-induced M1 macrophage polarization.

* Corresponding author.
** Corresponding author. CAS Key Laboratory of Molecular Imaging, Beijing Key Laboratory of Molecular Imaging, Institute of Automation, Chinese Academy of Sciences, Beijing, 100190, China.
*** Corresponding author. CAS Key Laboratory of Molecular Imaging, Beijing Key Laboratory of Molecular Imaging, Institute of Automation, Chinese Academy of Sciences, Beijing, 100190, China.
E-mail addresses: zsh_0615@163.com (S. Zhang), niniya731@163.com (Y. Zhang), 18112039@bjtu.edu.cn (P. Zhang), weizechen2019@ia.ac.cn (Z. Wei), ma_ming_rui@163.com (M. Ma), avigor@163.com (W. Wang), waynetong_301@163.com (W. Tong), tianf327@126.com (F. Tian), hui.hui@ia.ac.cn (H. Hui), jie.tian@ia.ac.cn (J. Tian), cyundai@vip.163.com (Y. Chen).
[1] These authors contributed equally to this work as co-first author.

https://doi.org/10.1016/j.heliyon.2023.e17314
Received 30 December 2022; Received in revised form 6 June 2023; Accepted 13 June 2023
Available online 14 June 2023

1. Introduction

Atherosclerosis is the major underlying mechanism of cardiovascular disease and the leading cause of death globally [1]. Despite exposure of the entire arterial tree to systemic risk factors such as hypercholesterolemia, hypertension, and hyperglycemia, a higher prevalence of atherosclerotic plaques is found at bifurcations than at linear regions [2,3]. Plaque rupture and erosion occur frequently near coronary bifurcations in patients with acute coronary syndromes [4–6]. Bifurcation lesions are a highly intriguing topic of interest in research, posing challenges stemming from the complex intervention strategies and multiple complications associated with their treatment [7,8].

The distribution of atherosclerotic plaques is spatially heterogeneous, mainly due to local hemodynamic factors [3]. Disturbed flow with low and oscillatory flow leads to monocyte infiltration into the intima and differentiation into macrophages in the early stages of atherosclerosis [9]. However, further research is necessary to gain additional insights into the roles of disturbed flow involving other aspects of the atherosclerotic process, such as persistent inflammation [10]. The chronic inflammatory response in the intimal layer of artery walls is a key contributor to atherosclerosis [11]. The balance of pro-inflammatory and anti-inflammatory mechanisms controls the atherosclerotic process [12]. Macrophages are the major inflammatory cells involved in the atherosclerotic process—especially M1 macrophages—which secrete inflammatory cytokines and matrix metalloproteinases to promote disease progression [13].

Plexin D1 (PLXND1) is a type I transmembrane protein involved in axonal guidance, tumor progression, and immunoregulation [14,15]. PLXND1 was recently identified as a force transducer that forms a mechano-complex with neuropilin-1 (NRP1) and vascular endothelial growth factor receptor 2 (VEGFR2) in endothelial cells to mediate shear stress, leading to differences in the distribution of atherosclerotic lesions between aortic arch and descending aorta at different disease stages in a mouse model of atherosclerosis [16]. Furthermore, PLXND1 and its ligand—semaphorin 3E (SEMA3E)—were highly expressed by macrophages in advanced atherosclerotic lesions [17]. The roles of PLXND1 in the initiation and progression of atherosclerotic plaques remain a topic of debate. Moreover, the distributions and corresponding functions of PLXND1 in atherosclerotic lesions at sites of disturbed flow are yet unclear. The aim of this study was to investigate the relationship between PLXND1 and atherosclerosis progression in bifurcations exposed to disturbed flow.

In this study, we established bifurcation lesions in ApoE$^{-/-}$ mice fed a high-fat diet (HFD) to evaluate the spatial distribution of PLXND1 and polarized macrophages, to link the disturbed pattern of blood flow. To further investigate the role of PLXND1 in disturbed flow-induced atherosclerosis, we co-cultured oxidized low-density lipoprotein (oxLDL)-treated THP-1-derived macrophages with human umbilical vein endothelial cells (HUVECs) exposed to different shear stress patterns *in vitro*. Our studies have demonstrated that PLXND1 plays a critical role in M1 macrophage polarization and SEMA3E-PLXND1 interaction enhances M1 macrophage polarization in disturbed flow fields at carotid bifurcations.

2. Methods

2.1. Atherosclerotic animal model

ApoE$^{-/-}$ mice [male, 6 weeks old, specific pathogen-free (SPF)] were purchased from Beijing Vital River Laboratory Animal Technology Co., Ltd. (Beijing, China, SCXK2016-0006). To establish the atherosclerosis model, mice were fed a HFD (15% fat, 1.25% cholesterol, 0.2% sodium cholate) for 0, 10, or 20 weeks after one week of acclimatization. They were housed in an SPF environment with free access to water and food. All studies involving mice were approved by the Institutional Animal Care and Use Committee of the Chinese PLA General Hospital (protocol numbers: 2021-X17-123) and conformed to the local and US National Institutes of Health guidelines for the Care and Use of Laboratory Animals.

2.2. Computational fluid dynamics (CFD) analysis

To obtain artery geometries, contrast-enhanced micro-computed tomography (CT) imaging (Quantum GX MicroCT Imaging System, PerkinElmer) was used. CT contrast agents (ExiTron nano 12000; MiltenyiBiotech) were intravenously administered at a dose of 5 μL/g body weight via the tail vein and scanned 30 min after injection. CT scanning was performed at 90 kV voltage, 88 μA current, 20 μm voxel size, high-resolution scan mode, and 14 min scan duration. The CT raw data were first processed by the Mimics Medical 21.0 (Materialise NV, Leuven, Belgium) software package. Bilateral carotid arteries were coarsely segmented using the automatic segmentation methods, namely the region growth and threshold methods. Subsequently, all the slices were refined by manual modification to further optimize the quality. The segmentation results were converted to the mesh model for finite element analysis using ANSYS Workbench (Release 19.0; ANSYS Inc. Canonsburg, PA, USA). The viscous model was solved by CFD using Fluent (Fluent 19.0, Ansys). Blood was assumed to be incompressible with fluid density of 1050 kg/m^3 and viscosity of 0.0035 kg/m•s. Vessel wall was assumed to be rigid. Average blood flow velocity of the common carotid arteries was measured by VisualSonics Vevo 2100 (Fujifilm VisualSonics, Inc. Toronto, Canada) and subsequently used as the inlet boundary condition. The pressure outlet at output region was set at zero. Wall shear stress (WSS) was then derived from the computed velocity field. WSS was computed by the formula: $\overrightarrow{WSS} = \overrightarrow{t} - (\overrightarrow{t} \bullet \overrightarrow{n})\overrightarrow{n}$, where $\overrightarrow{n}$ is the normal vector on the luminal surface of the blood vessel. Finally, after 200 iterations, the blood flow was calculated in 2 s, and the time step size was set to 0.1 s. Two points were selected at the bifurcations and common carotid arteries, respectively, to calculate their changes in WSS. WSS was normalized by dividing the mean value of WSS at 0.5 s interval.

2.3. Arteries harvest

Whole arterial trees were harvested after the mice had been fed a HFD for 0, 10, or 20 weeks. The mice were strongly anesthetized using 5% isoflurane, and then sacrificed by cervical dislocation and cardiac perfused with heparinized phosphate-buffered saline (PBS) and 4% paraformaldehyde sequentially. Arteries were isolated under a dissecting microscope. We defined the artery bifurcation region as the area with a diameter of 3 mm around the bifurcation carina. Arteries were separated from the arterial trees and fixed in 4% paraformaldehyde at 4 °C until further processing.

2.4. Histology and immunostaining

The fixed arteries were embedded in paraffin, and then 4-μm sections were mounted on glass slides. Hematoxylin and eosin (H&E) and immunofluorescence staining were performed following standard protocols [18]. For immunofluorescence staining, the following primary antibodies were used: PLXND1 (NBP1-33634, Novus), iNOS (ab283655, Abcam), Liver Arginase (ab239731, Abcam), F4/80 (ab300421, Abcam) and SEMA3E (AF3239, R&D Systems). The slides were scanned on a Pannoramic 250 system (3DHISTECH Ltd.), and images were analyzed using the Pannoramic Viewer software (3DHISTECH Ltd.). The percent fluorescent positive area was calculated as the fluorescent signal area divided by the entire intima area and quantified using the FIJI software (version 2.1.0/1.53c, National Institutes of Health, Bethesda, MD, USA).

2.5. Immunolabeling and clearing of arteries

Tissue clearing was performed as previously reported [19–21]. Fixed arteries were removed from 4 °C and kept at room temperature (RT) for 2 h. The arteries were then washed in PBS twice and dehydrated with 50%, 80% methanol in PBS and 100% methanol twice for 1 h each. Arteries were bleached using 5% H_2O_2 (1:5 dilution of 30% H_2O_2 with methanol) at 4 °C overnight. The rehydration process was performed using methanol twice, 80% methanol in dimethyl sulfoxide (DMSO) twice, and 80% and 50% methanol in PBS at RT for 1 h each. After washing twice with PBS plus 0.2% Triton X-100, the arteries were permeabilized in the solution containing 80% PBS, 20% DMSO, 0.2% Triton X-100, and 0.3 mol/L glycine at 37 °C overnight. Samples were then blocked at 37 °C for 3 d with blocking solution (85% PBS, 10% DMSO, 5% goat serum, and 2% Triton X-100). They were washed twice each hour with PBS supplemented with 0.2% Tween-20 and 10 μg/mL heparin (PTwH). Samples were next incubated with primary antibodies for PLXND1 (NBP1-33634, Novus) and iNOS (14-5920-82, Invitrogen) in PTwH and 5% DMSO at 37 °C for 3 d. Following washing 10 times with PTwH at each hour, the tissues were stained with Alexa Fluor 647-conjugated and Alexa Fluor 568-conjugated secondary antibodies (Invitrogen) for 3 d and finally washed with PTwH for 3 h 5 times. Samples embedded in 1% agar were dehydrated using graded dilutions (25%, 50%, 75%, and 100%) of methanol in PBS for 3 h per dilution at RT. Tissues were then optically cleared using BABB (1 part benzyl alcohol: 2 parts benzyl benzoate) overnight.

2.6. Image acquisition and analysis of light sheet fluorescent microscopy (LSFM) data

The samples were imaged by LSFM (Ultramicroscope II, LaVision Biotec, Bielefeld, Germany) with a 2.5 × objective lens (Mv PLAPO 2VC, Olympus). Excitation wavelengths included 488, 568, and 647 nm. The scanning z-step size was 5 μm. The Imaris software (Bitplane, Oxford Instruments Company) was utilized to perform sectioning and reconstruct three-dimensional (3D) projections of the arteries. To calculate the mean fluorescence value, the region of interest (ROI) of the plaque was first extracted by the threshold segmentation method. The sum of fluorescence intensity in the ROI of the plaque was then divided by the area of the plaque to determine the mean fluorescence value. The LSFM images were processed using the FIJI software. The ROIs of the plaque for both the PLXND1 and iNOS channels were determined to evaluate co-localization via Pearson's correlation coefficient (PCC) and Mander's overlap coefficient (MOC) of the plaque using the co-localization Finder plugin in FIJI.

2.7. Fluorescence molecular imaging

A PLXND1-targeted molecular probe was synthesized by conjugation of a single-domain antibody (A12) [22,23] and Cy5 fluorescent dyes (A12-Cy5; MerryBio Co., Ltd., Nanjing, China). *Ex vivo* imaging was conducted with the IVIS Spectrum imaging system (PerkinElmer, Waltham, MA, USA). Mice were euthanized by cervical dislocation to harvest the whole arterial trees and washed with PBS for *ex vivo* imaging 20 min after intravenous injection of the probe (200 μL, 90 μg). Relative fluorescence intensity was determined using a Cy5 filter channel. Images were captured and analyzed using the Living Image Software version 4.7.2 (Caliper Life Sciences). The bifurcation lesion site was manually marked and defined as the region of interest (ROI). The average fluorescence intensity within this ROI was then compared to the average intensity in the ROI of the same size taken from an adjacent region of the common carotid artery.

2.8. Cell culture

PUMC-HUVEC-T1s (hereafter referred to as HUVECs) and THP-1 cells were purchased from the Cell Resource Center, IBMS, CAMS/PUMC (Beijing, China). HUVECs were cultured in Dulbecco's modified Eagle medium with 10% fetal bovine serum (FBS). THP-1 cells were cultured in Roswell Park Memorial Institute 1640 medium with 10% FBS and differentiated into macrophages with 50 nM

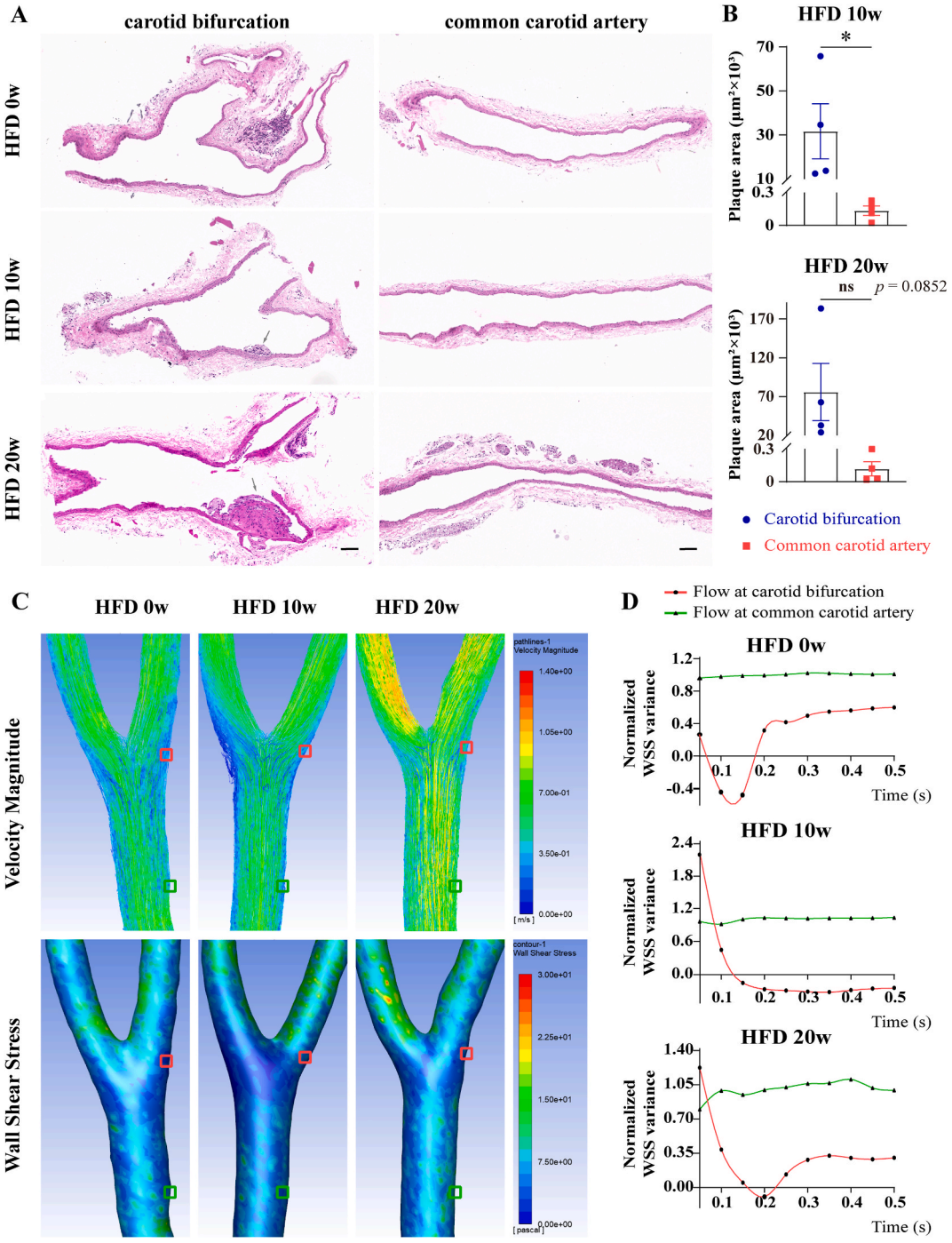

Fig. 1. The bifurcation of carotid artery differs from the linear region in hemodynamics and histology. (A) The sections of carotid bifurcation and common carotid artery from the same vessel were analyzed by H&E staining for indicating the presence or absence of atherosclerotic plaques in mice carotid arteries. Representative images of H&E staining are shown (scale bar, 100 μm). (B) The total plaque area of each slice was calculated. There were more lesions at carotid bifurcations than common carotid arteries. Data are shown as the mean ± SEM. $n = 4$. *$P < 0.05$, unpaired two-tailed Student's t tests. (C) Simulations of computational fluid dynamic (CFD) visualized and quantified the distribution of flow velocity and wall shear stress (WSS) in carotid arteries. The flow velocities were slower and the shear stress were lower on the lateral walls of carotid bifurcations than common carotid arteries. (D) The time traces were graphically displayed that is about the wall shear stress in the positions at carotid bifurcations or common carotid arteries on the side of the external carotid arteries indicated by red or green boxes in (C), respectively. WSS amplitudes demonstrate they are oscillating at bifurcations relative to those at linear regions. Graphs are representative of three independent samples. HFD, high-fat diet. (For interpretation of the references to colour in this figure legend, the reader is referred to the Web version of this article.)

phorbol-12-myristate 13-acetate (PMA, Sigma) for 48 h. Both cell types were maintained at 37 °C and 5% CO_2 atmosphere in a humidified incubator. To establish M1 or M2 macrophages, resting macrophages were differentiated via exposure to 100 ng/mL PMA for 48 h and then activated by lipopolysaccharide (LPS, 100 ng/mL, Sigma) and interferon-gamma (IFN-γ, 20 ng/mL, PeproTech) or by interleukin (IL)-4 (20 ng/mL, PeproTech) and IL-13 (20 ng/mL, PeproTech) stimulation for 24 h, respectively.

2.9. Generation of PLXND1-knockdown stable cells

For stable knockdown of PLXND1, THP-1 cells were transduced with short hairpin RNA (sh-PLXND1 and sh-Control) in lentiviral particles containing a green fluorescent protein (GFP). In brief, cells were cultured with short-hairpin-containing lentiviral supernatants in the presence of 5 μg/mL polybrene for 12 h. After 48 h, transduction efficiency was determined by fluorescence microscopy. After transfection, cells were treated with the indicated drugs for another 24 h. The transduced cells with lentivirus used in this study were obtained from Cyagen Biosciences Inc. (Suzhou, China). The shRNA sequence was 5′-CCAAGTGTTCCTCCCTTTATGCTCGAGCATAAAGGGAGGAACACTTGG-3′. The knockdown efficiency was routinely confirmed by quantitative reverse transcription polymerase chain reaction (qRT-PCR) [24]. The forward primer sequence was AATGGGCGGAACATCGTCAAG and the reverse primer sequence was CGAGACTGGTTGGAAACACAG. These transfected cells were further used for differentiation into macrophages.

2.10. Co-culture in a parallel-plate shear system

To further evaluate macrophage polarization under different shear stress conditions, we co-cultured 50 μg/mL oxLDL (IO1300, Solarbio)-treated THP-1-derived macrophages with HUVECs exposed to atherogenic oscillatory shear mimicking disturbed flow or atheroprotective laminar shear stress mimicking stable flow in a parallel-plate co-culture flow system for 24 h. The medium in the upper chamber was added with or without 500 ng/mL recombinant SEMA3E (3239-S3B, R&D). HUVEC-macrophage co-culture was conducted using cell culture inserts with a 0.4-μm pore size in a 6-well companion plate (Falcon 353090). The inserts were subsequently loaded into parallel-plate flow chambers and connected to a co-culture flow system (NK110-GPY; Shanghai Naturethink Life & Scientific Co., Ltd., Shanghai, China). The flow rate was regulated by a peristaltic pump (BT100-2J, LongerPump, Hebei, China) to generate steady laminar shear (12 dyn/cm^2) and oscillatory shear (0 ± 4 dyn/cm^2, 1 Hz) for 24 h.

2.11. Western blot analysis

Cells were washed twice with cold PBS, collected using cell scrapers and transferred to pre-chilled tubes. Collected cells were centrifuged at 500*g* for 5 min, and cell pellets were stored at −80 °C. Proteins were extracted from cell pellets using a lysis buffer for western blotting and their concentrations were measured by bicinchoninic acid assay (Applygen Technologies, P1511). Western blotting was performed according to standard procedures [25]. The primary antibodies were anti-PLXND1 (NBP1-33634, Novus), anti-SEMA3E (AF3239, R&D Systems), anti-iNOS (ab283655, Abcam), anti-CD206 (ab125028, Abcam), anti-CD163 (ab156769, Abcam), anti-Liver Arginase (ab133543, Abcam), anti-STAT1 (phospho Y701) (ab109457, Abcam), anti-STAT1 (ab109320, Abcam), anti-STAT6 (phospho Y641) (ab263947, Abcam), anti-STAT6 (ab32520, Abcam) and anti-GAPDH (ab9485, Abcam) acted as an internal control. Western blots were quantified using the FIJI software. Uncropped Western blot gels are available in the Supplementary Information section.

2.12. Statistical analyses

All statistical analyses and graphical representations were performed using GraphPad Prism 9.2.0 (GraphPad Software, San Diego, CA, USA). Data are presented as mean ± SEM. Unpaired or paired two-tailed Student's *t* tests were used to analyze quantitative data of two groups. For multiple-group comparisons, quantitative data were analyzed by one-way analysis of variance and Bonferroni's post-hoc tests. A *P* value less than 0.05 was considered significant.

3. Results

3.1. The bifurcations of carotid arteries exposed to disturbed flow become atheroprone

H&E staining in both the carotid bifurcations and common carotid arteries showed that atherosclerotic plaques mainly appeared at arterial bifurcations at 10 and 20 weeks after HFD feeding (Fig. 1A and B). As hemodynamic disturbed flow is associated with susceptibility to atherosclerosis, CFD of carotid arteries was performed in $ApoE^{-/-}$ mice. These simulations of flow patterns showed slower flow velocity and lower shear stress levels on the lateral walls of the carotid bifurcations than the common carotids in the same vessels (Fig. 1C). Moreover, WSS at bifurcations was oscillating, while the laminar flow at the common carotid arteries was steady (Fig. 1D). These observations suggest that bifurcation lesion development is linked to disturbed flow at carotid bifurcations.

3.2. PLXND1 is primarily expressed in M1 macrophages in carotid bifurcation lesions

To clarify the role of PLXND1 in atherosclerosis, we first examined its expression in different regions of $ApoE^{-/-}$ mouse carotid at 10 and 20 weeks after HFD feeding. Immunofluorescence staining of tissue sections showed that the differential expression of PLXND1

in intra-lesion M1 and M2 macrophages. The high expression level of PLXND1 co-localized predominantly with inducible nitric oxide synthase (iNOS)$^{+}$M1 macrophages relative to arginase 1 (ARG1)$^{+}$M2 macrophages (Fig. 2A and B). These results indicated that PLXND1 was expressed more in M1 macrophages rather than M2 macrophages at bifurcation lesions. The endothelial marker CD31 was detected simultaneously with PLXND1 and iNOS in sections of bifurcation plaques at HFD for 10 weeks (Fig. S1A). Unlike iNOS, which co-localized with PLXND1 in plaques, PLXND1 co-staining with CD31 showed no significant co-localization by confocal imaging. We also detected HUVECs exposed to different flow patterns when they were co-cultured with macrophages *in vitro*. The expression of PLXND1 protein levels were not elevated under oscillatory shear stress condition (Fig. S1B). These results indicate that PLXND1 was expressed mainly in M1 macrophages rather than in endothelial cells at bifurcation lesions exposed to disturbed flow.

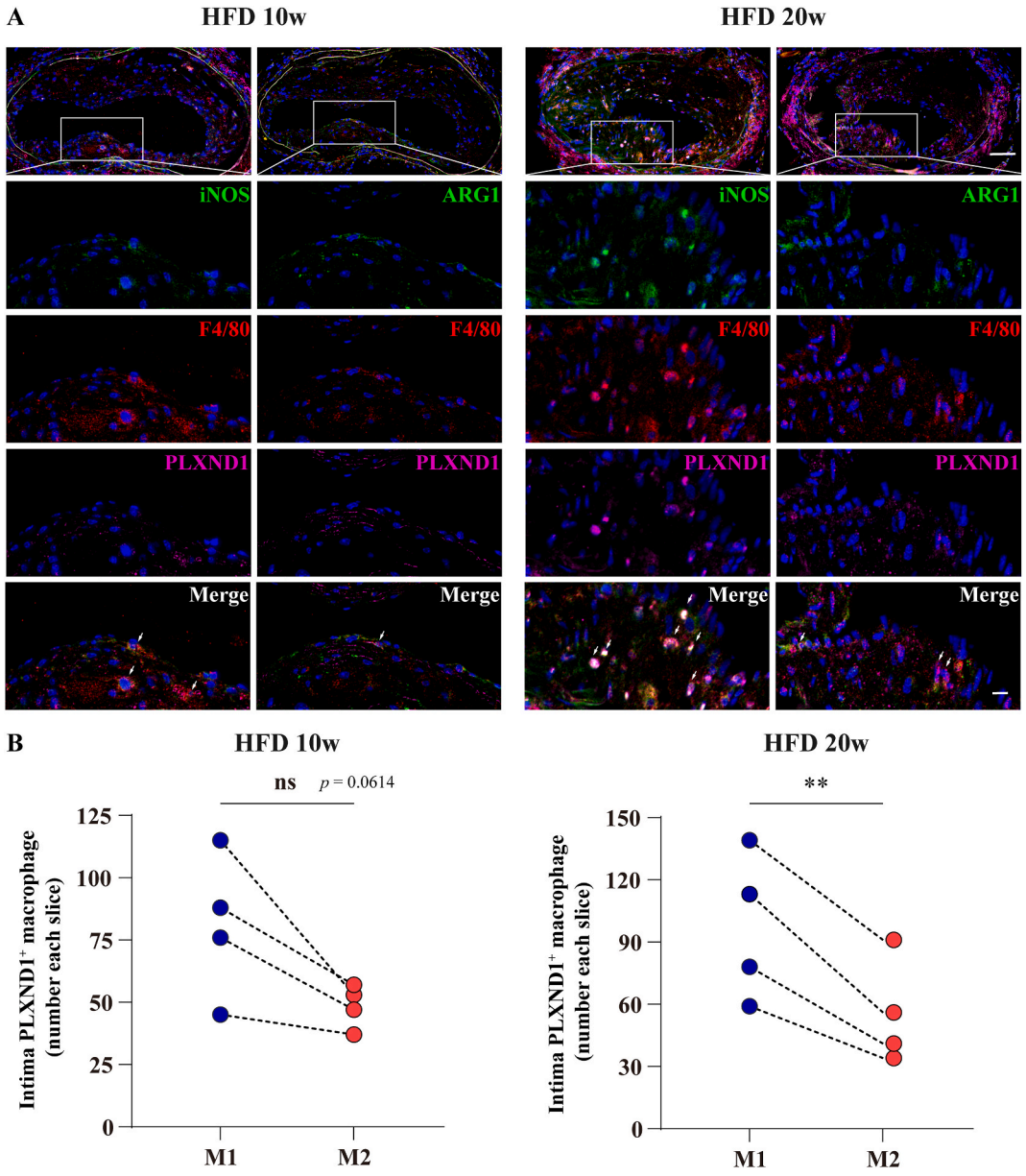

Fig. 2. M1 macrophages express more PLXND1 than M2 macrophages in bifurcation lesions of ApoE$^{-/-}$ mice after 10 weeks and 20 weeks of high fat diet. (A) Adjacent sections of carotid bifurcation lesions were used to examine M1 and M2 macrophages by immunofluorescence staining separately. Immunofluorescence staining was performed with iNOS (green) or ARG1 (green), F4/80 (red), PLXND1 (pink), and DAPI (blue). Representative images are shown on the top (scale bar, 100 μm) and enlarged images of inserts are shown below (scale bar, 20 μm). (B) Intima PLXND1 + iNOS + F4/80 + M1 macrophages and PLXND1 + ARG1 + F4/80 + M2 macrophages were presented as number each slice. PLXND1 was expressed more in M1 macrophages rather than M2 macrophages. $n = 4$. $^{**}P < 0.01$, paired two-tailed t tests. HFD, high-fat diet. (For interpretation of the references to colour in this figure legend, the reader is referred to the Web version of this article.)

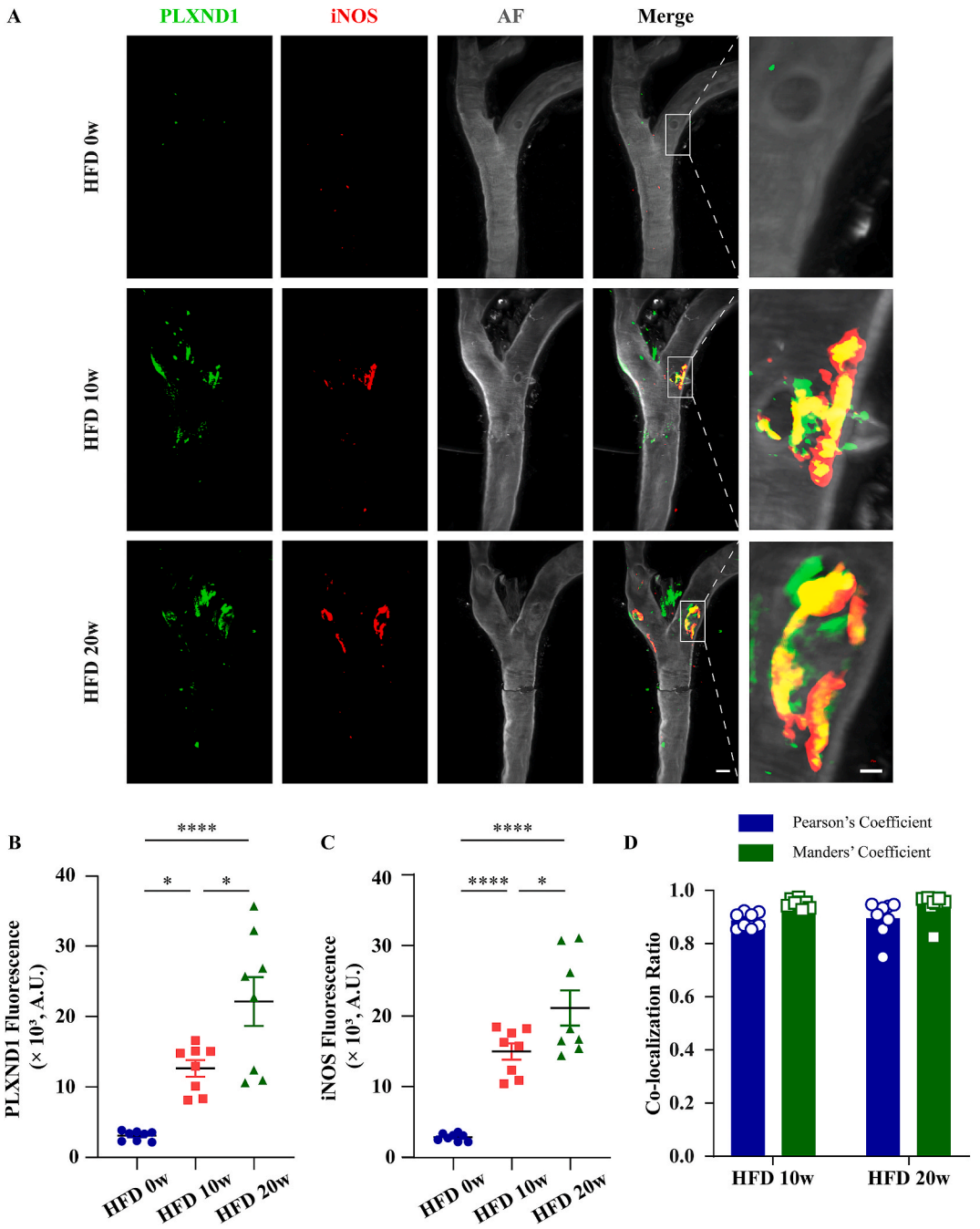

Fig. 3. PLXND1 expression level and location in process of atherosclerosis at bifurcations are evaluated by three-dimensional reconstruction. (A) 3D projections of PLXND1 (green) and iNOS (red) with autofluorescence at carotid bifurcations were depicted during atherosclerosis development by tissue clearing and light-sheet imaging. Representative images are shown (scale bar, 100 μm). Enlarged images of inserts are shown at right (scale bar, 10 μm). (B) Quantitative analyses of PLXND1 fluorescence of plaques show PLXND1 expression level increased by high-fat diet over time ($n = 4$ mice; two carotid arteries/mice). (C) Quantitative analyses of iNOS fluorescence of plaques show iNOS expression level increased by high fat diet over time ($n = 4$ mice; two carotid arteries/mice). (D) Co-localization of PLXND1 with iNOS in plaques at bifurcations was quantitatively analyzed ($n = 4$ mice; two carotid arteries/mice). Data are shown as the mean ± SEM. *$P < 0.05$, ****$P < 0.0001$, one-way ANOVA with Bonferroni's post-hoc tests. AF, autofluorescence. HFD, high-fat diet. (For interpretation of the references to colour in this figure legend, the reader is referred to the Web version of this article.)

3.3. The expression of PLXND1 in M1 macrophages is related to progression of bifurcation lesions

To better visualize and quantify PLXND1 in different disease stages, we used 3D whole-mount imaging by LSFM with tissue clearing to explore the relationship between PLXND1 and progression of bifurcation lesions. After HFD feeding for 10 weeks, 3D LSFM imaging of cleared mouse carotid arteries demonstrated the presence of PLXND1 and iNOS in the plaques located on the lateral walls of carotid bifurcations (Fig. 3A), in contrast to the patterns observed in 0-week HFD group (Fig. 3B and C); moreover, their distribution exhibited co-localization (PCC = 0.8881, MOC = 0.9516; Fig. 3D). After HFD feeding for 20 weeks, the expression levels of PLXND1 and iNOS were higher than those after 10 weeks of HFD feeding (Fig. 3B and C); furthermore, they were co-localized in enlarged plaques (PCC = 0.8965, MOC = 0.9432; Fig. 3C). These data depict changes of PLXND1 and iNOS protein levels at bifurcations in 3D and indicate that PLXND1 in M1 macrophages is associated with disease progression.

3.4. Fluorescent molecular probes targeting PLXND1 allow in vivo detection of plaques

To investigate the ability to monitor the disease *in vivo* via targeting PLXND1, we constructed fluorescent molecular probes targeting PLXND1, A12-Cy5, that A12 specifically recognizing PLXND1 has been reported [22,23]. Twenty minutes after injecting the tail veins with A12-Cy5, high fluorescence signals appeared in the atherosclerotic regions with disturbed blood flow, such as at the carotid bifurcations, whereas the arteries from ApoE$^{-/-}$ mice fed the HFD for 0 week showed extremely low fluorescence signals in these areas (Fig. 4A). Tissue clearing and LSFM imaging were then performed to confirm the accumulation of fluorescent probes inside the atherosclerotic plaque (Fig. 4B). In addition, we quantitatively analyzed the ratio of fluorescence intensity between carotid bifurcations and common carotid arteries. The mean fluorescence intensity values at bifurcations were ~1.65-fold higher after HFD feeding for 10 weeks and were ~1.99-fold higher after HFD feeding for 20 weeks compared with those for the common carotid arteries. The ratio increased significantly at HFD for 10 weeks compared to HFD for 0 week; a significant difference was also found at HFD for 20 weeks relative to that detected in the group fed the HFD for 10 weeks (Fig. 4C). These data show that probes targeting PLXND1 provide a good means to monitor the progression of bifurcation lesions.

3.5. PLXND1 modulates LPS/IFN-γ-induced M1 macrophages polarization in vitro

To explore the mechanism by which PLXND1 expression is regulated in atherosclerotic plaques at bifurcations, we used THP-1 cell-derived macrophages for further *in vitro* analysis. THP-1 monocyte cells differentiated into macrophages and further polarized to M1 or M2 types. To confirm the phenotype of these macrophages, the macrophage markers iNOS (M1 marker), CD206 (M2 marker), CD163

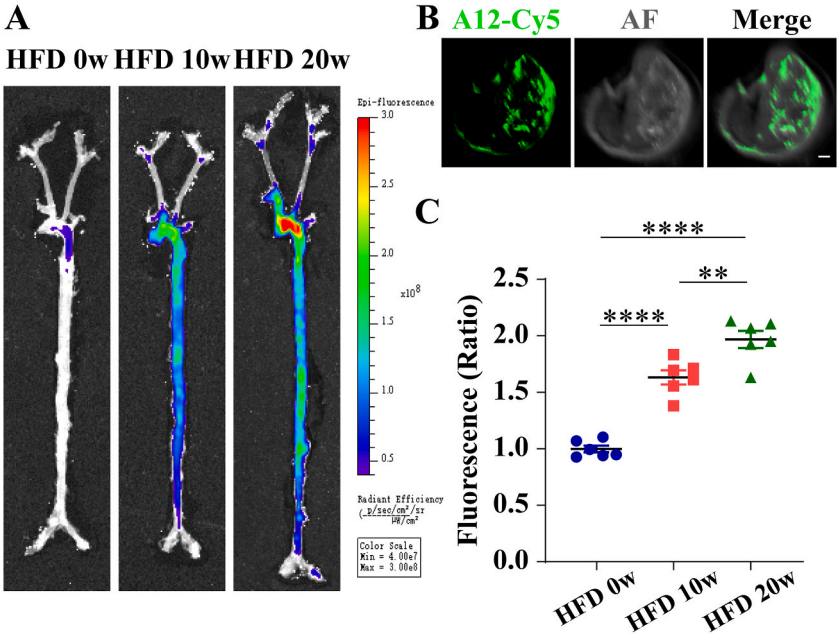

Fig. 4. Carotid bifurcation lesions are detected by probes targeting PLXND1. (A) Fluorescence imaging of isolated arteries from ApoE$^{-/-}$ mice were performed after intravenous injection of A12-Cy5, the molecular probes specific for PLXND1. A12-Cy5 showed stronger signals in carotid bifurcation lesions than common carotid arteries. (B) Arteries were conducted tissue clearing and light-sheet imaging. The images show that fluorescent probes accumulate inside the plaques (scale bar, 1 mm). (C) The ratio of fluorescent intensity between carotid bifurcation and common carotid artery were quantitatively analyzed at HFD 0w, 10w, 20w (n = 3 mice; two carotid arteries/mice). Data are shown as the mean ± SEM. $^{**}P < 0.01$, $^{****}P < 0.0001$, one-way ANOVA with Bonferroni's post-hoc tests. AF, autofluorescence. HFD, high-fat diet.

(M2 marker) and ARG1 (M2 marker) were detected by western blotting (Fig. 5A). Besides these, we examined signal transducer and activator of transcription 1 (STAT1) and STAT6 [26,27], transcription factors which are linked to M1 and M2 macrophage polarization, respectively (Fig. 5B). In addition, PLXND1 expression increased in M1 macrophages following stimulation by LPS and IFN-γ (Fig. 5A, B and 5C). To further explore the role of PLXND1 in regulating macrophage polarization, knockdown and control THP-1 cell lines were generated. The knockdown efficiency of PLXND1 was validated by western blotting (Fig. 5D and E). We also used qRT-PCR to confirm that the efficiency of knockdown was 34% (data not shown). We then evaluated the expression of iNOS, the M1 macrophage marker in response to LPS and IFN-γ stimulation. We found that PLXND1 knockdown THP-1-derived macrophages have significantly reduced expression of iNOS by LPS and IFN-γ compared to control cell lines (Fig. 5F and G). These data point to polarization of macrophages toward a M1 phenotype are modulated by PLXND1.

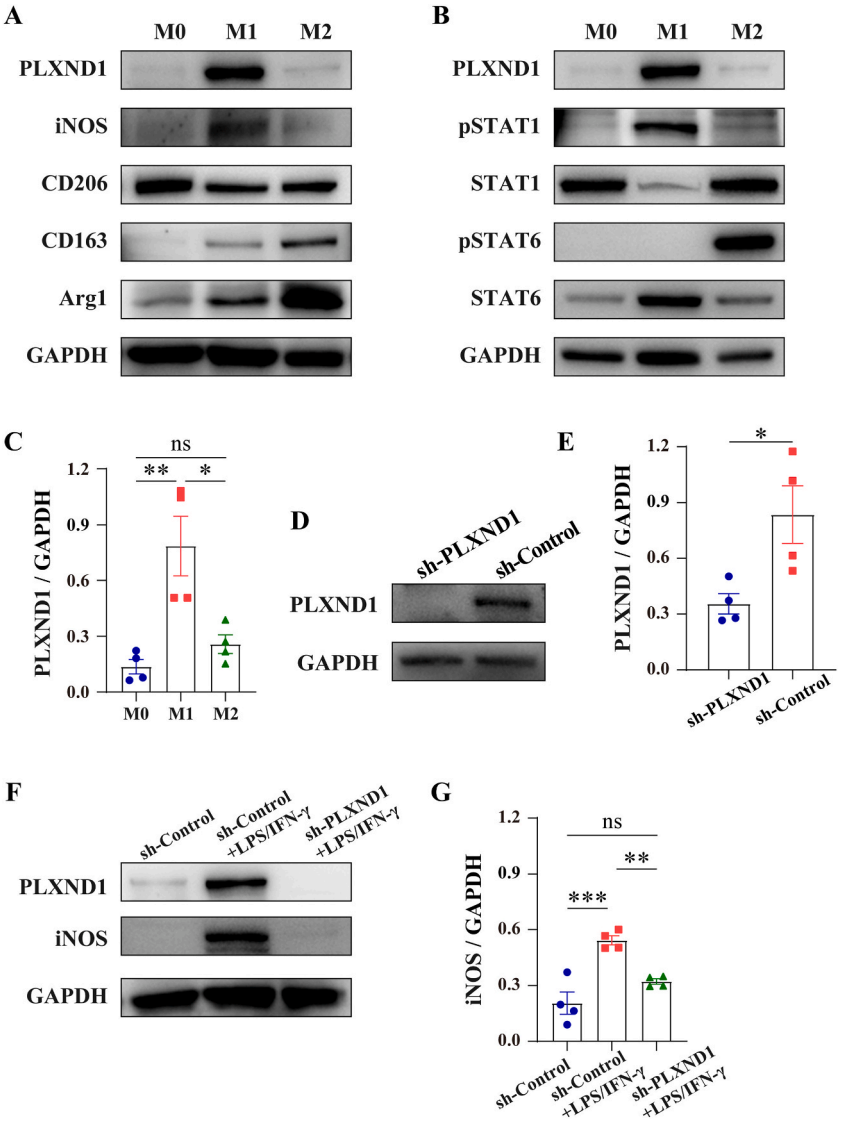

Fig. 5. PLXND1 regulates LPS/IFN-γ-induced M1 macrophages polarization. (A) THP-1 cells were differentiated into macrophages, and then polarized to M1 or M2 macrophages by LPS/IFN-γ or IL-4/IL-13. Representative Western blots of PLXND1, iNOS (M1 marker), CD206 (M2 marker), CD163 (M2 marker), ARG1 (M2 marker) and GAPDH in M0, M1 and M2 type macrophages are shown. (B) Representative Western blots of PLXND1, p-STAT1/STAT1, p-STAT6/STAT6 and GAPDH in M0, M1 and M2 type macrophages are shown. (C) Quantitative analysis of PLXND1 protein expression demonstrates the highest level of PLXND1 protein in M1 macrophage. (D) THP-1 cells were transfected with shRNA to knockdown PLXND1. The knockdown efficiency was verified by western blotting (WB) and quantification of WB in (E). (F) THP-1 cells were transfected with sh-Control or sh-PLXND1 and further differentiated into macrophages via PMA. THP-1-derived macrophages were then incubated with or without LPS/IFN-γ. Representative Western blots of PLXND1, iNOS, and GAPDH are shown. (G) iNOS protein expression was quantitatively analyzed. Knockdown of PLXND1 attenuates the induction of iNOS, the M1 polarization marker in macrophages treated with LPS/IFN-γ. Data are shown as the mean ± SEM. $n = 4$. *$P < 0.05$, **$P < 0.01$, ***$P < 0.001$, one-way ANOVA with Bonferroni's post-hoc test or unpaired two-tailed Student's t tests.

3.6. PLXND1 mediates oscillatory shear stress-induced M1 polarization in vitro

In order to investigate the effects of shear stress on macrophage polarization, THP-1-derived macrophages were treated with oxLDL and co-cultured with HUVECs for 24 h (Fig. 6A). In comparison with atheroprotective laminar shear stress and no mechanical stimulation, oscillatory shear stress (mimicking disturbed flow) applied significantly increased protein expression levels of PLXND1 and iNOS (Fig. 6B–D). To further verify the effect of PLXND1 on macrophage polarization in this model, shear stress-treated HUVECs were co-cultured with oxLDL-treated macrophages which had been differentiated from THP-1 with or without PLXND1 knockdown via PMA. The results of western blotting analyses revealed that knockdown of PLXND1 in macrophages co-cultured with oscillatory shear stress-treated HUVECs led to the significantly reduced expression of iNOS, compared with control (Fig. 6E and F). These results indicate that knocking down PLXND1 inhibits M1 macrophage polarization induced by co-culture with oscillatory shear stress-treated HUVECs.

3.7. SEMA3E-PLXND1 enhances M1 polarization under oscillatory shear

PLXND1 has been identified as a receptor that transduce signals in response to SEMA3E during inflammatory responses [28]. Hence, we investigated whether SEMA3E participates in the regulation of macrophage polarization. To confirm SEMA3E localization in bifurcation lesions, sections from ApoE$^{-/-}$ mice fed for 10 weeks were stained for SEMA3E, PLXND1, iNOS and F4/80. Immunofluorescence staining revealed that SEMA3E and PLXND1 were co-localized in M1 macrophages (Fig. 7A). To further study the effect of SEMA3E on macrophage polarization induced by co-culture with shear stress-treated HUVECs, we treated macrophages with or without recombinant SEMA3E (rSEMA3E). Treatment with rSEMA3E caused a significant increase expression of iNOS in macrophages

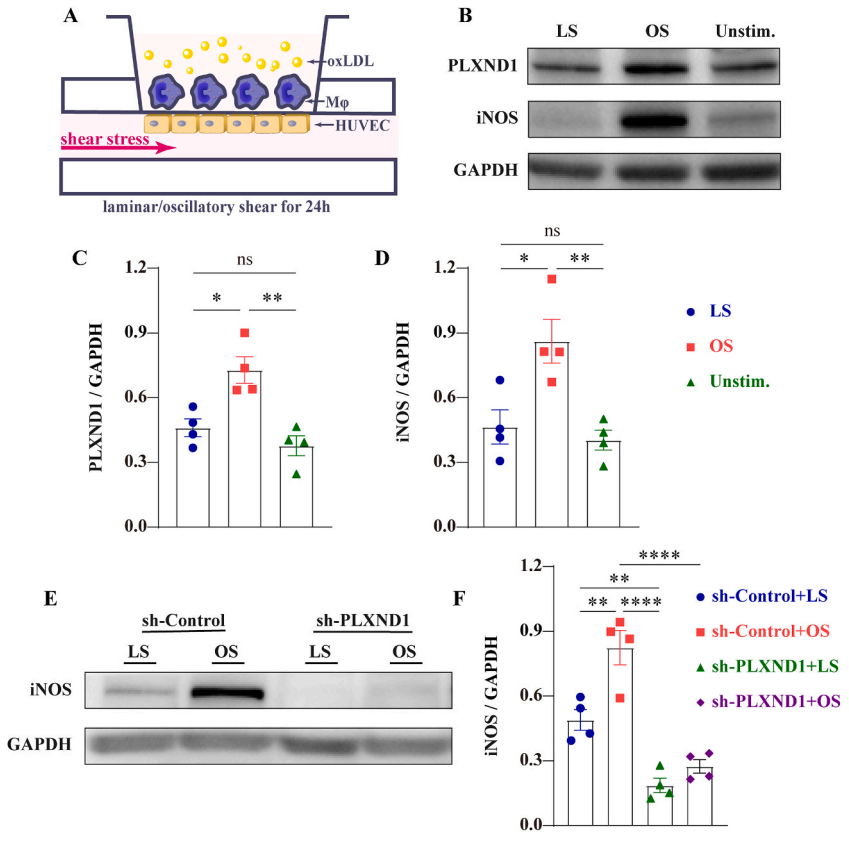

Fig. 6. PLXND1 regulates M1 macrophages polarization induced by oscillatory shear stress. (A) A schematic drawing of the experiment is outlined. THP-1-derived macrophages were treated with oxLDL and co-cultured with HUVECs exposed to laminar shear or oscillatory shear for 24 h in a parallel-plate shear flow system. (B) Macrophages were co-cultured with HUVECs exposed to laminar shear or oscillatory shear, or just incubated with media (Unstim.). Representative Western blots of PLXND1, iNOS (M1 macrophage marker) and GAPDH in macrophages are shown (C, D). PLXND1 and iNOS protein expressions were quantitatively analyzed from (B). These results show that oscillatory shear stress induced M1 macrophage polarization and increased PLXND1 expression at the same time. (E) THP-1-derived macrophages transfected with sh-Control or sh-PLXND1 were co-cultured with HUVECs exposed to laminar shear or oscillatory shear. The M1 macrophage marker, iNOS was detected by WB and quantification of WB in (F). Knockdown of PLXND1 attenuates M1 macrophage polarization induced by oscillatory shear stress. Data are shown as the mean ± SEM. $n = 4$. *$P < 0.05$, **$P < 0.01$, ****$P < 0.0001$, one-way ANOVA with Bonferroni's post-hoc tests. LS, laminar shear. OS, oscillatory shear.

induced by co-culture with oscillatory shear stress-treated HUVECs (Fig. 7B and C). To evaluate the cellular mechanism of the increased expression of iNOS induced by SEMA3E, we investigated whether this effect was through the interaction with PLXND1. PLXND1 knockdown strongly reduced the elevated iNOS levels in macrophages induced by treatment with rSEMA3E when they were co-cultured with oscillatory shear stress-treated HUVECs (Fig. 7D and E). Taken together, our findings suggest that SEMA3E enhances M1 macrophage polarization through the interaction with PLXND1 and PLXND1 is critical in mediating M1 macrophage polarization induced by co-culture with oscillatory shear stress-treated HUVECs.

4. Discussion

In this study, we explored the role of PLXND1 in M1 macrophage polarization in bifurcation lesions. The high expression level of PLXND1 is primarily expressed on macrophages with M1 phenotypes in bifurcation lesions of ApoE$^{-/-}$ mice, closely related to atherosclerotic disease progression. The ligand of PLXND1, SEMA3E, was also co-localized with PLXND1 in M1 macrophages. PLXND1 was distributed at the lateral walls of carotid bifurcations where the shear stress was low and oscillatory. PLXND1 knockdown reduced

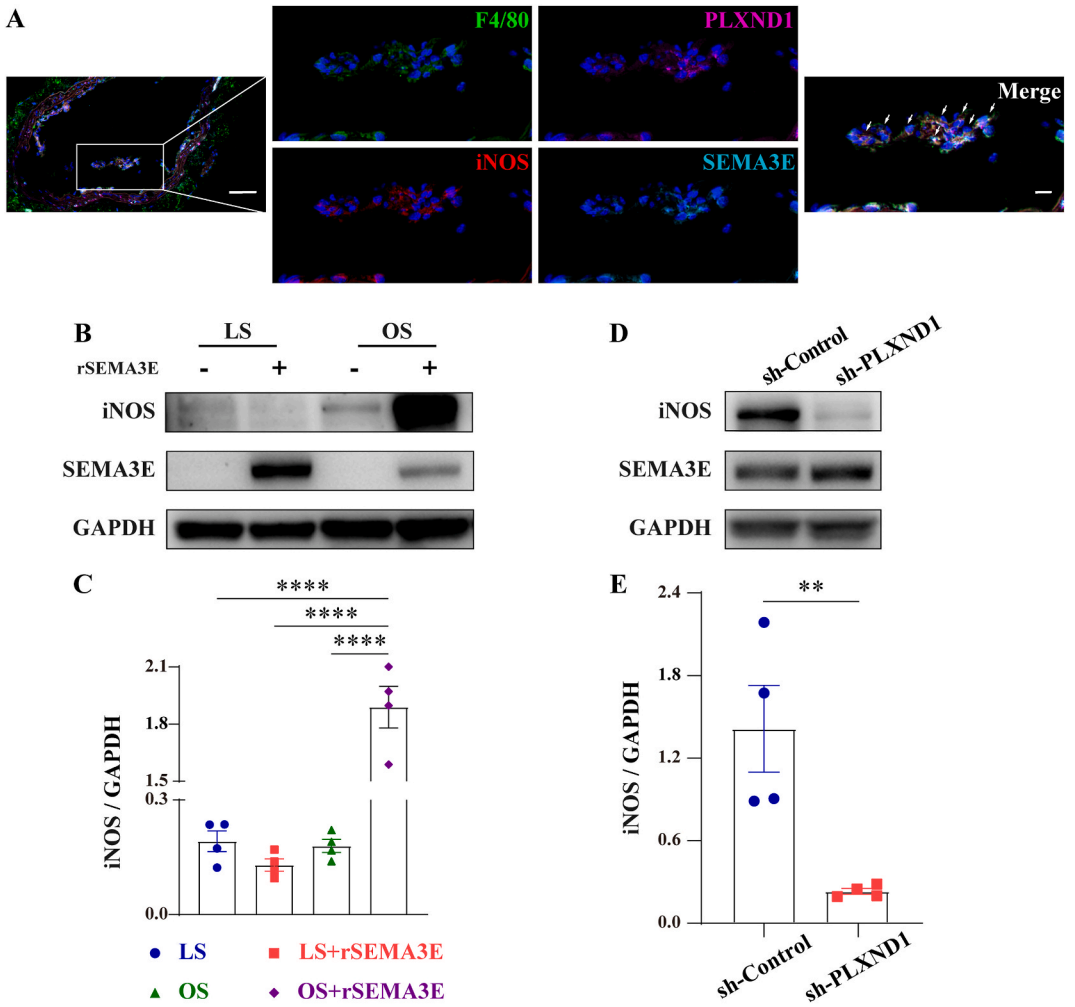

Fig. 7. Oscillatory shear enhances M1 polarization by SEMA3E-PLXND1. (A) Immunofluorescence staining of bifurcation lesions was performed with iNOS (red), F4/80 (green), PLXND1 (pink), SEMA3E (green blue) and DAPI (blue). Representative images are shown on the left (scale bar, 100 μm) and enlarged images of inserts are shown on the right (scale bar, 20 μm). (B) THP-1-derived macrophages were co-cultured with HUVECs exposed to laminar shear or oscillatory shear in treatment with or without 500 ng/mL recombinant SEMA3E (rSEMA3E). Immunoblot analysis of iNOS are shown. (C) Quantitative analysis showed SEMA3E enhanced M1 polarization under oscillatory shear. (D) THP-1-derived macrophages transfected with sh-Control or sh-PLXND1 were co-cultured with HUVECs exposed to oscillatory shear in treatment with rSEMA3E. The expression of iNOS was analyzed by WB. (E) Quantitative analysis showed iNOS expression was significantly lower in sh-PLXND1 cells. Data are shown as the mean ± SEM. $n = 4$. $^{**}P < 0.01$, $^{****}P < 0.0001$, one-way ANOVA with Bonferroni's post-hoc tests or unpaired two-tailed Student's t tests. LS, laminar shear. OS, oscillatory shear. (For interpretation of the references to colour in this figure legend, the reader is referred to the Web version of this article.)

disturbed flow-induced M1 macrophage polarization. These findings demonstrate that PLXND1 participates in the regulation of disturbed flow-induced macrophage polarization and the spatially heterogeneous distribution of plaques; furthermore, SEMA3E enhances M1 macrophage polarization via interaction with PLXND1.

Arterial bifurcations are susceptible to atherosclerosis and are characterized by higher-risk features compared to non-bifurcation lesions [4–6]. The etiology of the heterogeneous spatial distributions of atherosclerotic lesions is incompletely resolved. It is known that the locations of disturbed flow are associated with the predilection sites of atherosclerotic plaques [29]. Previous studies have shown that disturbed flow promotes endothelial dysfunction, causing the subsequent development of atherosclerosis [30–33]. The ensuing inflammation is another hallmark of atherosclerosis, which is characterized by the predominance of an M1 macrophage phenotype in the plaque, accompanied by the hypersecretion of inflammatory cytokines and matrix metalloproteinases [13]. Low and oscillatory WSS may influence plaque formation by facilitating an atherosclerosis-promoting hemodynamic environment, especially at the lateral walls of carotid bifurcations on one side of the external carotid artery [34,35]. WSS has also been shown to be strongly correlated with macrophage infiltration at carotid artery bifurcations in mouse atherosclerosis models [36]. Another study showed that low shear stress in mice induced M1 macrophage polarization by the upregulation of multiple pro-inflammatory chemokines and cytokines [37]. By ligating three out of four branches of the left carotid artery, the blood flow becomes more disturbed and M1 macrophages increase with the production of pro-inflammatory cytokines [38]. In the present study, we explored the relationship between M1 macrophages and flow patterns in atherosclerotic plaques at bifurcations. We visualized shear stress information from the carotid arteries during the development of atherosclerosis using CFD simulations. The results showed that the low and oscillatory shear stress was located at carotid bifurcations, which is consistent with previous findings [36,39]. LSFM affords quantitative analysis and 3D imaging of protein and cell localization in the native structural environment for large and irregular vessels [19,20]. Visualization of the distribution of M1 macrophages provided by LSFM of the carotid arteries in their entirety demonstrated that M1 macrophage-rich plaques were located in the disturbed flow areas. Our study revalidates that the number of pro-inflammatory M1 macrophage is closely related to disturbed flow in spatial dimensions, which is an important contributor to bifurcation lesions.

This study focused on PLXND1, which is expressed in various types of cells such as macrophages, adipocytes, and nerve cells [14,15]. However, the exact roles of PLXND1 in atherogenesis remain unclear and are probably complex. As the ligand of PLXND1, SEMA3E inhibits macrophage migration, thereby contributing to macrophage retention in atherosclerosis progression [17]. Another study found that PLXND1-SEMA3E signaling played a key role in suppressing the proliferation and migration of vascular smooth muscle cells during neointima formation [40]. Furthermore, PLXND1 is a direct mechanoreceptor that forms a mechanosensory complex with NRP1 and VEGFR2 in endothelial cells, which then transmits the shear stress signal to regulate the site-specific distribution of atherosclerotic lesions [16]. To explore the underlying mechanisms between PLXND1 and atherosclerotic plaques triggered by disturbed flow, we evaluated the distribution of PLXND1 in spatial and temporal dimensions. 3D visualization of the carotid arteries showed that PLXND1 was highly expressed at the bifurcation lesions and its expression level increased substantially as the lesions progressed. Our CFD results demonstrate that the shear stress is low and oscillating at carotid bifurcations where PLXND1 proteins are enriched. We also performed molecular-targeted imaging of atherosclerosis using fluorescence molecular imaging [41] to display the distribution of PLXND1 in atherosclerosis-prone mice. These results confirmed that PLXND1 appeared in regions of disturbed flow. Immunofluorescence analysis of tissue slices showed that PLXND1 was mainly distributed in M1 macrophages. In addition to this, the quantitative 3D data sets of LSFM strengthened the reliability of data showing that elevated levels of PLXND1 highly co-localized with iNOS, the M1 macrophage marker in bifurcation lesions. These findings were further supported by *in vitro* experiments. PLXND1 was highly expressed in polarized M1 macrophages. To mimic the microenvironment of bifurcation lesions, we established a shear stress-treated HUVECs and oxLDL-treated macrophages co-culture system and found that the expression level of PLXND1 in polarized M1 macrophages were increased when co-cultured HUVECs treated with oscillatory shear stress, which was consistent with the results of our *in vivo* experiment. Additionally, this study revealed that PLXND1 deficiency in macrophages restrained macrophage polarization into the pro-inflammatory M1 phenotype not only in response to LPS and IFN-γ, but also co-cultured with oscillatory shear stress-treated HUVECs.

As the ligand of PLXND1, SEMA3E is a member of the semaphorin family of axon guidance regulators; its dysregulation is linked to diverse pathologies, including cancers, cardiovascular disorders, and autoimmune diseases [42,43]. SEMA3E promotes adipose tissue inflammation by inducing PLXND1-positive macrophage infiltration in dietary obesity [28]. PLXND1 deficiency reduces triglyceride storage and visceral fat volumes, leading to improved insulin resistance [44,45]. The SEMA3E-PLXND1 axis participates in chronic metabolic and inflammatory diseases. Moreover, serum SEMA3E levels are positively correlated with the severity of atherosclerosis [46,47]. Our preliminary results showed that SEMA3E was concomitant with the presentation of PLXND1 in M1 macrophages of bifurcation lesions. *In vitro* experiments demonstrated that SEMA3E promoted more iNOS expressed in macrophages which induced by co-culture with oscillatory shear stress-treated HUVECs and SEMA3E exerted this effect via PLXND1. These findings indicate that SEMA3E may be involved in PLXND1-mediated macrophage polarization in atherosclerotic lesions at arterial bifurcations exposed to disturbed flow.

There are several limitations of this study. First, although *in vitro* experiments were carried out in the simulated local microenvironment of bifurcation lesions, the components of atherosclerotic plaque *in vivo* are more complex than those *in vitro.* Further investigations on the mechanism by which PLXND1 exerts its regulatory effect should be performed in macrophage-specific PLXND1-knockout mice. Second, we found oscillatory shear stress induced M1 macrophage polarization via PLXND1, but the crosstalk between endothelial cells and macrophages is unknown which need to be further addressed. More related detail is needed to clarify the role of PLXND1 in atherosclerosis induced by disturbed flow.

5. Conclusion

In conclusion, the present study supports that PLXND1 in M1 macrophages is related to the heterogeneous spatial distribution of atherosclerotic plaques and accounted for the initiation and progression of bifurcation lesions. PLXND1 mediates M1 macrophage polarization induced by disturbed flow. SEMA3E contributes to PLXND1-mediated macrophage polarization toward M1 macrophage phenotype under oscillatory shear stress condition. This study linking hemodynamic, macrophage polarization and PLXND1 would improve our understanding of bifurcation lesions and may provide a potential therapeutic candidate for treating cardiovascular diseases.

Ethics approval

All studies involving mice were approved by the Institutional Animal Care and Use Committee of the Chinese PLA General Hospital (protocol numbers: 2021-X17-123).

Funding statement

This work was supported by the National Key Research and Development Program of China 2017YFA0700401; the National Natural Science Foundation of China 81827808, 81730050, 81870178, 81800221, 62027901, 81527805, and 81671851; the CAS Youth Innovation Promotion Association 2018167 and CAS Key Technology Talent Program; the Project of High-Level Talents Team Introduction in Zhuhai City (Zhuhai HLHPTP201703). The authors would like to acknowledge the instrumental and technical support of Multimodal Biomedical Imaging Experimental Platform, Institute of Automation, Chinese Academy of Sciences.

Author contribution statement

Suhui Zhang: Conceived and designed the experiments; Performed the experiments; Analyzed and interpreted the data; Wrote the paper.

Yingqian Zhang and Hui Hui: Conceived and designed the experiments; Analyzed and interpreted the data; Wrote the paper.

Peng Zhang and Zechen Wei: Performed the experiments; Analyzed and interpreted the data.

Mingrui Ma, Wei Wang, Wei Tong and Feng Tian: Performed the experiments.

Jie Tian and Yundai Chen: Conceived and designed the experiments; Contributed reagents, materials, analysis tools or data.

Data availability statement

Data will be made available on request.

Declaration of competing interest

The authors declare that they have no known competing financial interests or personal relationships that could have appeared to influence the work reported in this paper.

Appendix A. Supplementary data

Supplementary data to this article can be found online at https://doi.org/10.1016/j.heliyon.2023.e17314.

References

[1] G.A. Roth, G.A. Mensah, V. Fuster, The global burden of cardiovascular diseases and risks: a compass for global action, J. Am. Coll. Cardiol. 76 (2020) 2980–2981, https://doi.org/10.1016/j.jacc.2020.11.021.

[2] G. Nakazawa, S.K. Yazdani, A.V. Finn, M. Vorpahl, F.D. Kolodgie, R. Virmani, Pathological findings at bifurcation lesions, J. Am. Coll. Cardiol. 55 (2010) 1679–1687, https://doi.org/10.1016/j.jacc.2010.01.021.

[3] U. Morbiducci, A.M. Kok, B.R. Kwak, P.H. Stone, D.A. Steinman, J.J. Wentzel, Atherosclerosis at arterial bifurcations: evidence for the role of haemodynamics and geometry, Thromb. Haemostasis 115 (2016) 484–492, https://doi.org/10.1160/th15-07-0597.

[4] J. Dai, L. Xing, H. Jia, Y. Zhu, S. Zhang, S. Hu, L. Lin, L. Ma, H. Liu, M. Xu, et al., In vivo predictors of plaque erosion in patients with ST-segment elevation myocardial infarction: a clinical, angiographical, and intravascular optical coherence tomography study, Eur. Heart J. 39 (2018) 2077–2085, https://doi.org/10.1093/eurheartj/ehy101.

[5] D.M. Leistner, N. Krankel, D. Meteva, Y.S. Abdelwahed, C. Seppelt, B.E. Stahli, H. Rai, C. Skurk, A. Lauten, H.C. Mochmann, et al., Differential immunological signature at the culprit site distinguishes acute coronary syndrome with intact from acute coronary syndrome with ruptured fibrous cap: results from the prospective translational OPTICO-ACS study, Eur. Heart J. 41 (2020) 3549–3560, https://doi.org/10.1093/eurheartj/ehaa703.

[6] M. Araki, T. Soeda, H.O. Kim, V. Thondapu, M. Russo, O. Kurihara, H. Shinohara, Y. Minami, T. Higuma, H. Lee, et al., Spatial distribution of vulnerable plaques: comprehensive in vivo coronary plaque mapping, JACC Cardiovasc. Imaging 13 (2020) 1989–1999, https://doi.org/10.1016/j.jcmg.2020.01.013.

[7] G. Di Gioia, J. Sonck, M. Ferenc, S.L. Chen, I. Colaiori, E. Gallinoro, T. Mizukami, M. Kodeboina, S. Nagumo, D. Franco, et al., Clinical outcomes following coronary bifurcation PCI techniques: a systematic review and network meta-analysis comprising 5,711 patients, JACC Cardiovasc. Intervent. 13 (2020) 1432–1444, https://doi.org/10.1016/j.jcin.2020.03.054.

[8] F. Burzotta, J.F. Lassen, T. Lefèvre, A.P. Banning, Y.S. Chatzizisis, T.W. Johnson, M. Ferenc, S. Rathore, R. Albiero, M. Pan, et al., Percutaneous coronary intervention for bifurcation coronary lesions: the 15(th) consensus document from the European Bifurcation Club, EuroIntervention 16 (2021) 1307–1317, https://doi.org/10.4244/eij-d-20-00169.

[9] P. Marchio, S. Guerra-Ojeda, J.M. Vila, M. Aldasoro, V.M. Victor, M.D. Mauricio, Targeting early atherosclerosis: a focus on oxidative stress and inflammation, Oxid. Med. Cell. Longev. 2019 (2019), 8563845, https://doi.org/10.1155/2019/8563845.

[10] Y.S. Chatzizisis, A.U. Coskun, M. Jonas, E.R. Edelman, C.L. Feldman, P.H. Stone, Role of endothelial shear stress in the natural history of coronary atherosclerosis and vascular remodeling: molecular, cellular, and vascular behavior, J. Am. Coll. Cardiol. 49 (2007) 2379–2393, https://doi.org/10.1016/j.jacc.2007.02.059.

[11] P. Libby, Inflammation in atherosclerosis, Nature 420 (2002) 868–874, https://doi.org/10.1038/nature01323.

[12] M. Bäck, A. Yurdagul, I. Tabas, K. Öörni, P.T. Kovanen, Inflammation and its resolution in atherosclerosis: mediators and therapeutic opportunities, Nat. Rev. Cardiol. (2019), https://doi.org/10.1038/s41569-019-0169-2.

[13] I. Tabas, K.E. Bornfeldt, Macrophage phenotype and function in different stages of atherosclerosis, Circ. Res. 118 (2016) 653–667, https://doi.org/10.1161/CIRCRESAHA.115.306256.

[14] C.M. Gay, T. Zygmunt, J. Torres-Vazquez, Diverse functions for the semaphorin receptor PlexinD1 in development and disease, Dev. Biol. 349 (2011) 1–19, https://doi.org/10.1016/j.ydbio.2010.09.008.

[15] S. Vivekanadhan, D. Mukhopadhyay, Divergent roles of Plexin D1 in cancer, Biochim. Biophys. Acta Rev. Canc 1872 (2019) 103–110, https://doi.org/10.1016/j.bbcan.2019.05.004.

[16] V. Mehta, K.L. Pang, D. Rozbesky, K. Nather, A. Keen, D. Lachowski, Y. Kong, D. Karia, M. Ameismeier, J. Huang, et al., The guidance receptor plexin D1 is a mechanosensor in endothelial cells, Nature 578 (2020) 290–295, https://doi.org/10.1038/s41586-020-1979-4.

[17] A. Wanschel, T. Seibert, B. Hewing, B. Ramkhelawon, T.D. Ray, J.M. van Gils, K.J. Rayner, J.E. Feig, E.R. O'Brien, E.A. Fisher, K.J. Moore, Neuroimmune guidance cue Semaphorin 3E is expressed in atherosclerotic plaques and regulates macrophage retention, Arterioscler. Thromb. Vasc. Biol. 33 (2013) 886–893, https://doi.org/10.1161/ATVBAHA.112.300941.

[18] A.T. Feldman, D. Wolfe, Tissue processing and hematoxylin and eosin staining, Methods Mol. Biol. 1180 (2014) 31–43, https://doi.org/10.1007/978-1-4939-1050-2_3.

[19] T. Becher, D.F. Riascos-Bernal, D.J. Kramer, V.M. Almonte, J. Chi, T. Tong, G.H. Oliveira-Paula, I. Koleilat, W. Chen, P. Cohen, N.E.S. Sibinga, Three-dimensional imaging provides detailed atherosclerotic plaque morphology and reveals angiogenesis after carotid artery ligation, Circ. Res. 126 (2020) 619–632, https://doi.org/10.1161/circresaha.119.315804.

[20] N.E. Buglak, J. Lucitti, P. Ariel, S. Maiocchi, F.J. Miller, E.S.M. Bahnson, Light sheet fluorescence microscopy as a new method for unbiased three-dimensional analysis of vascular injury, Cardiovasc. Res. 117 (2021) 520–532, https://doi.org/10.1093/cvr/cvaa037.

[21] W. Wang, Y. Zhang, H. Hui, W. Tong, Z. Wei, Z. Li, S. Zhang, X. Yang, J. Tian, Y. Chen, The effect of endothelial progenitor cell transplantation on neointimal hyperplasia and reendothelialisation after balloon catheter injury in rat carotid arteries, Stem Cell Res. Ther. 12 (2021) 99, https://doi.org/10.1186/s13287-021-02135-w.

[22] I. Roodink, J. Raats, B. van der Zwaag, K. Verrijp, B. Kusters, H. van Bokhoven, M. Linkels, R.M. de Waal, W.P. Leenders, Plexin D1 expression is induced on tumor vasculature and tumor cells: a novel target for diagnosis and therapy? Cancer Res. 65 (2005) 8317–8323, https://doi.org/10.1158/0008-5472.Can-04-4366.

[23] M.F. Debets, W.P. Leenders, K. Verrijp, M. Zonjee, S.A. Meeuwissen, I. Otte-Höller, J.C. van Hest, Nanobody-functionalized polymersomes for tumor-vessel targeting, Macromol. Biosci. 13 (2013) 938–945, https://doi.org/10.1002/mabi.201300039.

[24] T. Nolan, R.E. Hands, S.A. Bustin, Quantification of mRNA using real-time RT-PCR, Nat. Protoc. 1 (2006) 1559–1582, https://doi.org/10.1038/nprot.2006.236.

[25] J.J. Bass, D.J. Wilkinson, D. Rankin, B.E. Phillips, N.J. Szewczyk, K. Smith, P.J. Atherton, An overview of technical considerations for Western blotting applications to physiological research, Scand. J. Med. Sci. Sports 27 (2017) 4–25, https://doi.org/10.1111/sms.12702.

[26] H. Iwata, C. Goettsch, A. Sharma, P. Ricchiuto, W.W. Goh, A. Halu, I. Yamada, H. Yoshida, T. Hara, M. Wei, et al., PARP9 and PARP14 cross-regulate macrophage activation via STAT1 ADP-ribosylation, Nat. Commun. 7 (2016), 12849, https://doi.org/10.1038/ncomms12849.

[27] W. Cai, X. Dai, J. Chen, J. Zhao, M. Xu, L. Zhang, B. Yang, W. Zhang, M. Rocha, T. Nakao, et al., STAT6/Arg1 promotes microglia/macrophage efferocytosis and inflammation resolution in stroke mice, JCI Insight 4 (2019), https://doi.org/10.1172/jci.insight.131355.

[28] I. Shimizu, Y. Yoshida, J. Moriya, A. Nojima, A. Uemura, Y. Kobayashi, T. Minamino, Semaphorin3E-Induced inflammation contributes to insulin resistance in dietary obesity, Cell Metabol. 18 (2013) 491–504, https://doi.org/10.1016/j.cmet.2013.09.001.

[29] C. Hahn, M.A. Schwartz, Mechanotransduction in vascular physiology and atherogenesis, Nat. Rev. Mol. Cell Biol. 10 (2009) 53–62, https://doi.org/10.1038/nrm2596.

[30] G. Douglas, V. Mehta, A. Al Haj Zen, I. Akoumianakis, A. Goel, V.S. Rashbrook, L. Trelfa, L. Donovan, E. Drydale, S. Chuaiphichai, et al., A key role for the novel coronary artery disease gene JCAD in atherosclerosis via shear stress mechanotransduction, Cardiovasc. Res. 116 (2020) 1863–1874, https://doi.org/10.1093/cvr/cvz263.

[31] D. Qu, L. Wang, M. Huo, W. Song, C.W. Lau, J. Xu, A. Xu, X. Yao, J.J. Chiu, X.Y. Tian, Y. Huang, Focal TLR4 activation mediates disturbed flow-induced endothelial inflammation, Cardiovasc. Res. 116 (2020) 226–236, https://doi.org/10.1093/cvr/cvz046.

[32] B. Li, J. He, H. Lv, Y. Liu, X. Lv, C. Zhang, Y. Zhu, D. Ai, c-Abl regulates YAPY357 phosphorylation to activate endothelial atherogenic responses to disturbed flow, J. Clin. Investig. 129 (2019) 1167–1179, https://doi.org/10.1172/jci122440.

[33] S.E. Basehore, S. Bohlman, C. Weber, S. Swaminathan, Y. Zhang, C. Jang, Z. Arany, A.M. Clyne, Laminar flow on endothelial cells suppresses eNOS O-GlcNAcylation to promote eNOS activity, Circ. Res. 129 (2021) 1054–1066, https://doi.org/10.1161/circresaha.121.318982.

[34] D. De Wilde, B. Trachet, N. Debusschere, F. Iannaccone, A. Swillens, J. Degroote, J. Vierendeels, G.R.Y. De Meyer, P. Segers, Assessment of shear stress related parameters in the carotid bifurcation using mouse-specific FSI simulations, J. Biomech. 49 (2016) 2135–2142, https://doi.org/10.1016/j.jbiomech.2015.11.048.

[35] D. De Wilde, B. Trachet, G. De Meyer, P. Segers, The influence of anesthesia and fluid-structure interaction on simulated shear stress patterns in the carotid bifurcation of mice, J. Biomech. 49 (2016) 2741–2747, https://doi.org/10.1016/j.jbiomech.2016.06.010.

[36] D. De Wilde, B. Trachet, G.R.Y. De Meyer, P. Segers Shear, Stress metrics and their relation to atherosclerosis: an in vivo follow-up study in atherosclerotic mice, Ann. Biomed. Eng. 44 (2016) 2327–2338, https://doi.org/10.1007/s10439-015-1540-z.

[37] A.N. Seneviratne, J.E. Cole, M.E. Goddard, I. Park, Z. Mohri, S. Sansom, I. Udalova, R. Krams, C. Monaco, Low shear stress induces M1 macrophage polarization in murine thin-cap atherosclerotic plaques, J. Mol. Cell. Cardiol. 89 (2015) 168–172, https://doi.org/10.1016/j.yjmcc.2015.10.034.

[38] H. Merino, S. Parthasarathy, D.K. Singla, Partial ligation-induced carotid artery occlusion induces leukocyte recruitment and lipid accumulation–a shear stress model of atherosclerosis, Mol. Cell. Biochem. 372 (2013) 267–273, https://doi.org/10.1007/s11010-012-1468-7.

[39] P. Hernández-López, M. Cilla, M. Martínez, E. Peña, Effects of the haemodynamic stimulus on the location of carotid plaques based on a patient-specific mechanobiological plaque atheroma formation model, Front. Bioeng. Biotechnol. 9 (2021), 690685, https://doi.org/10.3389/fbioe.2021.690685.

[40] J.H. Wu, Y. Li, Y.F. Zhou, J. Haslam, O.N. Elvis, L. Mao, Y.P. Xia, B. Hu, Semaphorin-3E attenuates neointimal formation via suppressing VSMCs migration and proliferation, Cardiovasc. Res. 113 (2017) 1763–1775, https://doi.org/10.1093/cvr/cvx190.

[41] R. Qiao, X. Huang, Y. Qin, Y. Li, T.P. Davis, C.E. Hagemeyer, M. Gao, Recent advances in molecular imaging of atherosclerotic plaques and thrombosis, Nanoscale 12 (2020) 8040–8064, https://doi.org/10.1039/d0nr00599a.

[42] A. Alamri, A. Soussi Gounni, S.K.P. Kung, View point: semaphorin-3E: an emerging modulator of natural killer cell functions? Int. J. Mol. Sci. 18 (2017) https://doi.org/10.3390/ijms18112337.

[43] A.A. Derijck, S. Van Erp, R.J. Pasterkamp, Semaphorin signaling: molecular switches at the midline, Trends Cell Biol. 20 (2010) 568–576, https://doi.org/10.1016/j.tcb.2010.06.007.

[44] J.E. Minchin, I. Dahlman, C.J. Harvey, N. Mejhert, M.K. Singh, J.A. Epstein, P. Arner, J. Torres-Vázquez, J.F. Rawls, Plexin D1 determines body fat distribution by regulating the type V collagen microenvironment in visceral adipose tissue, Proc. Natl. Acad. Sci. U.S.A. 112 (2015) 4363–4368, https://doi.org/10.1073/pnas.1416412112.

[45] A.E. Justice, T. Karaderi, H.M. Highland, K.L. Young, M. Graff, Y. Lu, V. Turcot, P.L. Auer, R.S. Fine, X. Guo, et al., Protein-coding variants implicate novel genes related to lipid homeostasis contributing to body-fat distribution, Nat. Genet. 51 (2019) 452–469, https://doi.org/10.1038/s41588-018-0334-2.

[46] R.R. Qin, M. Song, Y.H. Li, F. Wang, H.M. Zhou, M.H. Liu, M. Zhong, Y. Zhang, W. Zhang, Z.H. Wang, Association of increased serum Sema3E with TRIB3 Q84R polymorphism and carotid atherosclerosis in metabolic syndrome, Ann. Clin. Lab. Sci. 47 (2017) 47–51.

[47] M. Keller, V. Mirakaj, M. Koeppen, P. Rosenberger, Neuronal guidance proteins in cardiovascular inflammation, Basic Res. Cardiol. 116 (2021) 6, https://doi.org/10.1007/s00395-021-00847-x.